Some Simple Simulations of Thunderstorm Outflows

PATRICK T. HAERTEL, RICHARD H. JOHNSON, AND STEFAN N. TULICH

Department of Atmospheric Science, Colorado State University, Fort Collins, Colorado

(Manuscript received 30 November 1999, in final form 3 August 2000)

ABSTRACT

Three idealized simulations of thunderstorm outflows are presented. Each outflow is a response to an instantaneous low-level cooling. The vertical structures of the coolings differ as do the environments in which the outflows form, and consequently the dynamics of the outflows differ. One outflow is a gravity current, another is a gravity wave, and the third comprises both a gravity current and a gravity wave. The horizontal transport of mass is important for the advance of the gravity-current outflow, but not for the gravity wave outflow, and it is suggested that this is the defining dynamical distinction between the two outflows. The simulations are compared to observations and it is suggested that some outflows previously characterized as gravity currents may better fit the gravity wave or gravity current/wave archetypes. It is also noted that the gravity wave component of an outflow may be generated directly by low-level cooling in addition to the commonly suggested mechanism of the interaction of a gravity current with a stable layer.

1. Introduction

At low levels within thunderstorms air is cooled by the evaporation of rain and the melting of graupel and hail. In response to such cooling a circulation develops that includes subsidence in the vicinity of the cooling and diverging air near the surface beneath the cooling. The diverging low-level air is referred to as the thunderstorm outflow. The leading edge of the outflow, or gust front, often propagates tens of kilometers away from the storm.

The kinematic and thermodynamic properties of outflows have been observed using surface-, tower-, and sonde-based instruments in addition to Doppler radars. At the surface the passage of the gust front is accompanied by a wind shift, a pressure rise, and often a temperature fall (Charba 1974; Goff 1976; Wakimoto 1982; Doviak and Ge 1984; Mueller and Carbone 1987; Fulton 1990; Koch et al. 1991; Locatelli et al. 1998; May 1999). Soundings have revealed outflows to be cooler than their environments to depths of up to 4 km; in some cases the maximum temperature perturbation occurs near the surface while in other cases it is elevated by 1–2 km (Wakimoto 1982). Wind measurements taken from towers have shown that outflow winds are often the strongest just behind the gust front where speeds can reach 35 m s^{-1} (Charba 1974; Goff 1976), and Doppler radars have measured outflows to be 500–2000 m deep (Wakimoto 1982; Mueller and Carbone 1987; May 1999).

Many outflows have been characterized as gravity currents (Charba 1974; Goff 1976; Wakimoto 1982; Mueller and Carbone 1987; May 1999). Benjamin (1968) showed that when a gravity current is in a steady state the velocity c of the leading edge is related to its depth d some distance back from the leading edge by the following equation:

$$c = k\sqrt{g'd}, \tag{1}$$

where g' equals gravity times the ratio of the perturbation density to that of the environment, and $k = [(1 - \alpha)(2 - \alpha)/(1 + \alpha)]^{1/2}$, where α is the ratio of the depth of the gravity current to the depth of the fluid in which it is advancing. For thunderstorm outflows characterized as gravity currents, k has been observed to range from 0.71 to 1.25 (Charba 1974; Wakimoto 1982; Mueller and Carbone 1987), whereas the theoretical value appropriate for atmospheric gravity currents is $(2)^{1/2}$ (the limiting case as $\alpha \to 0$). Using numerical simulations Klemp et al. (1994) show that at least some of the difference between observed and theoretical values for k can be attributed to surface friction and mixing.

Some outflows have been characterized as combinations of gravity currents and gravity waves or bores (Doviak and Ge 1984; Fulton 1990; Koch et al. 1991; Locatelli et al. 1998) In each of these cases the bore or wave eventually outpaced the gravity current so that the pressure and wind perturbations associated with the former preceded those associated with the latter. The bores

Corresponding author address: Dr. Patrick T. Haertel, Department of Atmospheric Science, Colorado State University, Fort Collins, CO 80523-1371.
E-mail: haertel@atmos.colostate.edu

and waves were thought to have been generated by the gravity current interacting with a stable layer consistent with the laboratory simulations of Rottman and Simpson (1989).

In this paper we present three idealized simulations of thunderstorm outflows. The simulations are intended to illustrate some of the most fundamental outflow dynamics in a simple way, and are therefore carried out using idealized atmospheres that comprise two or three isentropic layers. One of the outflows is a gravity current, another is a gravity wave, and the third comprises both a gravity current and a gravity wave. After noting the characteristics of each kind of outflow and the limitations of the idealized simulations we consider published observations of outflows. We suggest that some outflows previously characterized as gravity currents may better fit the gravity wave or gravity current/wave archetypes. We also note that the gravity wave component of an outflow may be generated directly by low-level cooling rather than by the interaction of a gravity current with a stable layer.

2. The idealized model

a. Equations

We attempted to select the simplest model atmosphere that could illustrate the most fundamental difference between gravity-current and gravity wave outflows. We chose an atmosphere comprising isentropic layers. To understand the simplicity of such an atmosphere consider a layer of air with constant entropy. If viscosity and the Coriolis force are neglected and the pressure is hydrostatic then the horizontal acceleration of the air equals $c_p \nabla T$ where c_p is the specific heat at constant pressure, ∇ is the horizontal gradient operator (where height is the vertical coordinate), and T is temperature. Since the lapse rate equals g/c_p, a constant, this acceleration is independent of height. Therefore, if the horizontal flow is initially independent of height within the layer it will remain so. This means that for a given time at each horizontal position a single vector describes the horizontal flow for the entire layer, just as in the shallow water equations.

For the model atmosphere the inviscid adiabatic primitive equations reduce to the following system:

$$\frac{D_l u_l}{Dt} + \frac{\partial M_l}{\partial x} = 0, \tag{2}$$

$$\frac{D_l m_l}{Dt} + m_l \frac{\partial u_l}{\partial x} = 0, \tag{3}$$

$$M_l = \begin{cases} c_p \left(\dfrac{1}{m'} \displaystyle\sum_{k=1}^{L} m_k \right)^{\kappa} \theta_1 & \text{for } l = 1 \\ M_{l-1} + c_p \left(\dfrac{1}{m'} \displaystyle\sum_{k=l}^{L} m_k \right)^{\kappa} (\theta_l - \theta_{l-1}) & \\ \qquad\qquad \text{for } l = 2, \ldots, L, & \end{cases} \tag{4}$$

where l and k denote the layer, L is the number of layers, x is distance, t is time, $D_l/Dt = \partial/\partial t + u_l \partial/\partial x$, $m_l(x, t)$ is mass per unit area, $u_l(x, t)$ is horizontal velocity, θ_l is potential temperature, $M_l(x, t)$ is the Montgomery potential, m' is the reference value of mass per unit area, c_p is the specific heat of dry air at a constant pressure, and $\kappa = c_p/R$ where R is the gas constant for dry air. For the simulations presented here $L = 2$, 3, and $m' = p_0/g$ where $p_0 = 100$ kPa.

The system (2)–(4) is simple and yet robust. It may be thought of as a partially discrete form of the inviscid, adiabatic primitive equations. It contains no approximations beyond those of the latter, and it may be used to approximate continuously stratified hydrostatic inviscid atmospheric motions to arbitrary precision, much in the same way that a discrete Fourier transform may be used to approximate a continous Fourier transform. Systems like (2)–(4) have been used in surprisingly few studies. The authors are aware of only two other such studies: DeMaria and Pickle (1988) simulated the maturation of tropical cyclones using a model atmosphere that comprised three isentropic layers, and Tao (1994) used the isentropic-layers approach to study wave-mean flow interaction in the stratosphere.

b. Numerics

We developed a Lagrangian method for solving (2)–(4) using the shallow water equations. In this section we introduce the method in its shallow water form, present two test simulations, and then dicuss how the method is modified to apply to (2)–(4).

The nondimensional slab-symmetric shallow water equations are as follows:

$$\frac{Du}{Dt} + \frac{\partial h}{\partial x} = 0, \tag{5}$$

$$\frac{Dh}{Dt} + h \frac{\partial u}{\partial x} = 0, \tag{6}$$

where h is the height of the free surface, u is velocity, and $D/Dt = \partial/\partial t + u\partial/\partial x$. The Lagrangian method uses a different form of the continuity equation, which is easily derived from (6). Let $x_1(t)$ and $x_2(t)$ denote the positions of two points of water. Then using Leibniz's rule and (6) we have

$$\begin{aligned} \frac{d}{dt} \int_{x_1}^{x_2} h \, dx &= \int_{x_1}^{x_2} \frac{\partial h}{\partial t} \, dx - (hu)_{x_1} + (hu)_{x_2} \\ &= \int_{x_1}^{x_2} - \frac{\partial}{\partial x}(hu) \, dx - (hu)_{x_1} + (hu)_{x_2} \\ &= 0. \end{aligned} \tag{7}$$

In other words the integrated height between the two points remains constant with respect to time.

Consider a layer of water and let $x_1, \ldots, x_p$ be po-

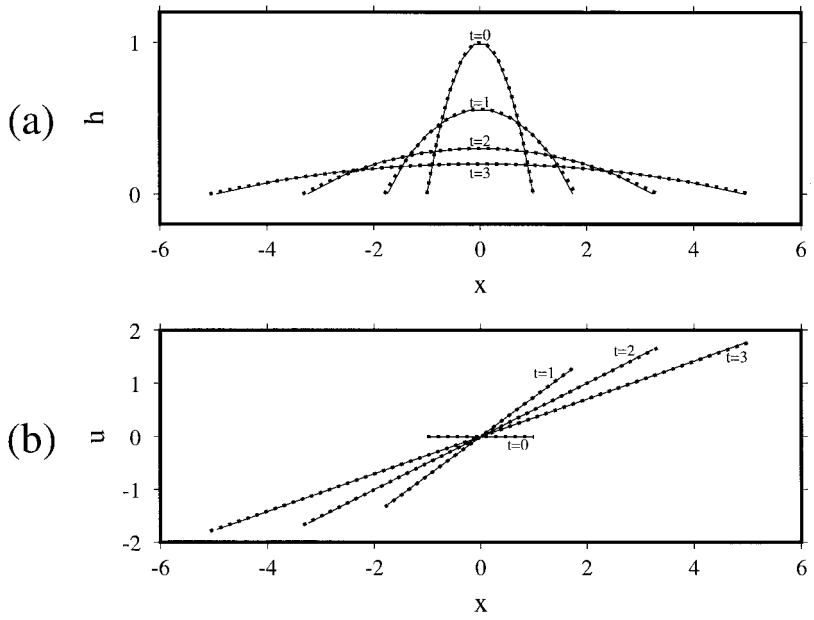

FIG. 1. Numerical (solid) and analytic (dotted) solutions for the spreading drop. (a) Height and (b) velocity.

sitions of points of water and let $u_1, \ldots, u_p$ be their velocities. Let $I_{i+1/2}$ denote the integrated height between x_i and x_{i+1}. Now suppose we do not know the height function and we wish to diagnose it from the positions and values of integrated height. We do know that the mean value of the height between x_i and x_{i+1} is $I_{i+1/2}/(x_{i+1} - x_i)$ and this is a reasonable estimate of the height at $x_{i+1/2} = (x_i + x_{i+1})/2$. Diagnosing h in this way and using forward time-differencing yields the following approximation of the system (5,7):

$$h^n_{i+1/2} = \frac{I_{i+1/2}}{x^n_{i+1} - x^n_i}, \tag{8}$$

$$\frac{u^{n+1}_i - u^n_i}{\Delta t} = -\frac{h^n_{i+1/2} - h^n_{i-1/2}}{x^n_{i+1/2} - x^n_{i-1/2}} + \frac{2\nu}{x^n_{i+1} - x^n_{i-1}}\left[\frac{u^n_{i+1} - u^n_i}{x^n_{i+1} - x^n_i} - \frac{u^n_i - u^n_{i-1}}{x^n_i - x^n_{i-1}}\right], \tag{9}$$

$$\frac{x^{n+1}_i - x^n_i}{\Delta t} = u^n_i. \tag{10}$$

Here n denotes the time level, Δt is the time step, and ν is kinematic diffusion, which is included for stability and smoothness. We use two kinds of boundary conditions: when the water has nonzero depth at a boundary we set the velocity to zero at the boundary, and when the water has zero depth at a boundary we diagnose h as zero at the fluid point closest to the boundary.

For the first test of the method we consider the evolution of a shallow drop of water that initially is motionless and has the shape of an inverted parabola with height 1 and radius 1. The drop maintains its parabolic shape and a linear velocity profile as it spreads with time (Frei 1993; Schär and Smolarkiewicz 1996). With $\Delta t = 0.01$, $\nu = 0$, and just 10 points the numerical method accurately reproduces the analytic solution (Fig. 1). For the second test we simulate gravity waves. Suppose there is a layer of water with basic state depth 1 and an initial Gaussian depth perturbation with amplitute 0.01 and radius 1. Under the linear approximation there is also an analytic solution for this initial condition. The height anomaly divides into two gravity waves, the right-moving (left-moving) wave having a velocity perturbation in phase (π radians out of phase) with the height perturbation. With 100 points (an inital point-spacing of 0.12), $\Delta t = 0.01$, and $\nu = 0$ the method also accurately reproduces this solution (Fig. 2).

For (2)–(4) the integrated mass between two points within a layer is time invariant, and we solve this system in the same way, but diagnosing mass for each layer instead of height. We then solve for the Montgomery potential for each layer at the same positions as mass using (4). Since the horizontal positions where mass is diagnosed vary from layer to layer, this requires interpolating the mass variable, and we use linear interpolation for that purpose. For the simulations presented here $\Delta t = 0.01$ s, the fluid points are initially spaced 50 m apart, and kinematic diffusion ranges between 1×10^3 and 4×10^3 m^2 s^{-1}.

3. Simulations

Thunderstorm outflows are atmospheric responses to cooling. Depending on the stratification of the atmosphere and the vertical structure of the cooling, the re-

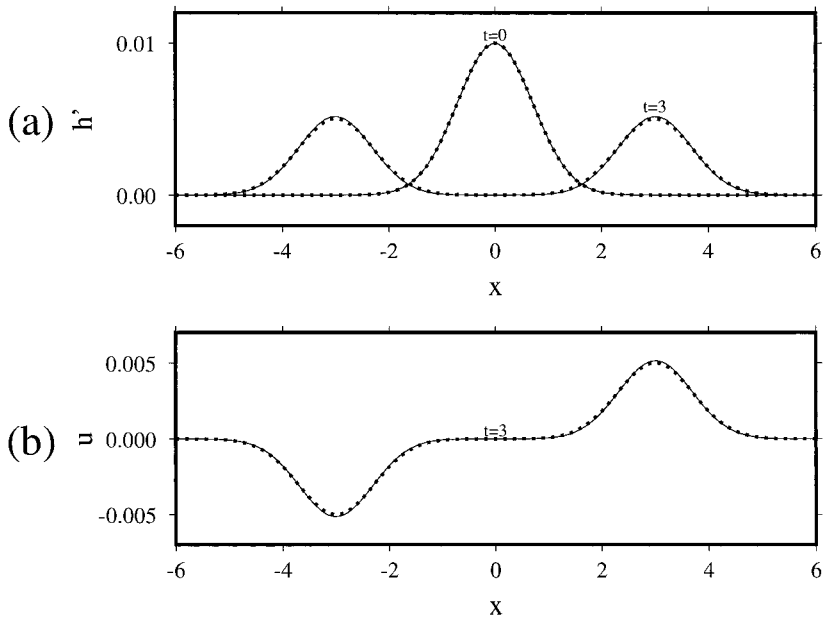

FIG. 2. Numerical (solid) and analytic (dotted) simulations of gravity waves. Perturbation (a) height and (b) velocity.

sponse may be a gravity current, a gravity wave, or a combination of the two. The simulations presented in this section illustrate each of these kinds of outflows in a simple form.

a. The gravity current

Consider an atmosphere that is isentropic with potential temperature $\theta_2 = 300$ K and a surface pressure of 1000 hPa. Suppose that a thunderstorm instantly cools a portion of the lower atmosphere to a potential temperature of $\theta_1 = 297$ K. Suppose that initially the cool air is motionless, and that it has a scale of 10 km and a maximum fractional column mass of one-fifth, which corresponds to a depth of about 1.9 km (Fig. 3a). The cool air subsides and spreads with time (Figs. 3b,c). At 10 min it has a scale of 25 km, a maximum depth of 670 m, and a rate of advance of 19 m s^{-1}. At each time the horizontal velocity function varies approximately linearly with respect to x within the cool air, and the depth curve resembles an inverted parabola, consistent with the analytic solution for the spread of a shallow drop of fluid (Fig. 1). Since the horizontal divergence is nearly constant within the cool air the vertical velocity varies little with respect to x, and the magnitude of the subsidence increases with height (Fig. 3b). The upper layer subsides above the center of the cool air and rises at the leading edges of the cool air (Figs. 3b,c).

It seems intuitive that the pool of cool, dense air should subside and spread with time, but intuition fails to answer the following question: the cooling does not alter the total mass above a given area, and therefore the surface pressure is initially unchanged, so what causes the initial motion of the cool air? To answer this question we consider how the cooling modifies the atmosphere as a whole. An atmosphere comprising a finite number of isentropic layers has a free upper surface, and the cooling locally reduces the height of this surface by up to 19 m (Fig. 3d). The perturbation in the depth of the atmosphere divides into two waves, which propagate away at a speed of $(RT_s)^{1/2} = 293$ m s^{-1} where T_s is the surface temperature. Once the waves transport most of the depth perturbation and mass deficit away, a surface high is left in their wake (Fig. 3e). The pressure gradient associated with this high causes the cool air to spread.

The fast-mode mass-adjustment of the real atmosphere to local cooling is somewhat different than that of the idealized model. In nature cooling at constant volume immediately produces low pressure consistent with the ideal gas law. The cooled air is then compressed as an acoustic wave propagates radially outward from the region of cooling. The result is the same, however, as a hydrostatic high is left beneath the cooled air.

The surface that bounds the cooler air is a material surface, and the two points at which this surface intersects the ground are gust fronts (Figs. 3b,c). We now consider the thermodynamic and kinematic changes that precede and accompany the passage of these gust fronts. Suppose an observer is standing at $x = 10$ km with a barometer, a thermometer, and an anemometer. At 30 s the observer measures a brief pressure drop (Fig. 4a) and weak temperature and wind perturbations (Figs. 4b,c) associated with the passage of the rapid-moving wave. This pressure drop is unrealistically intense be-

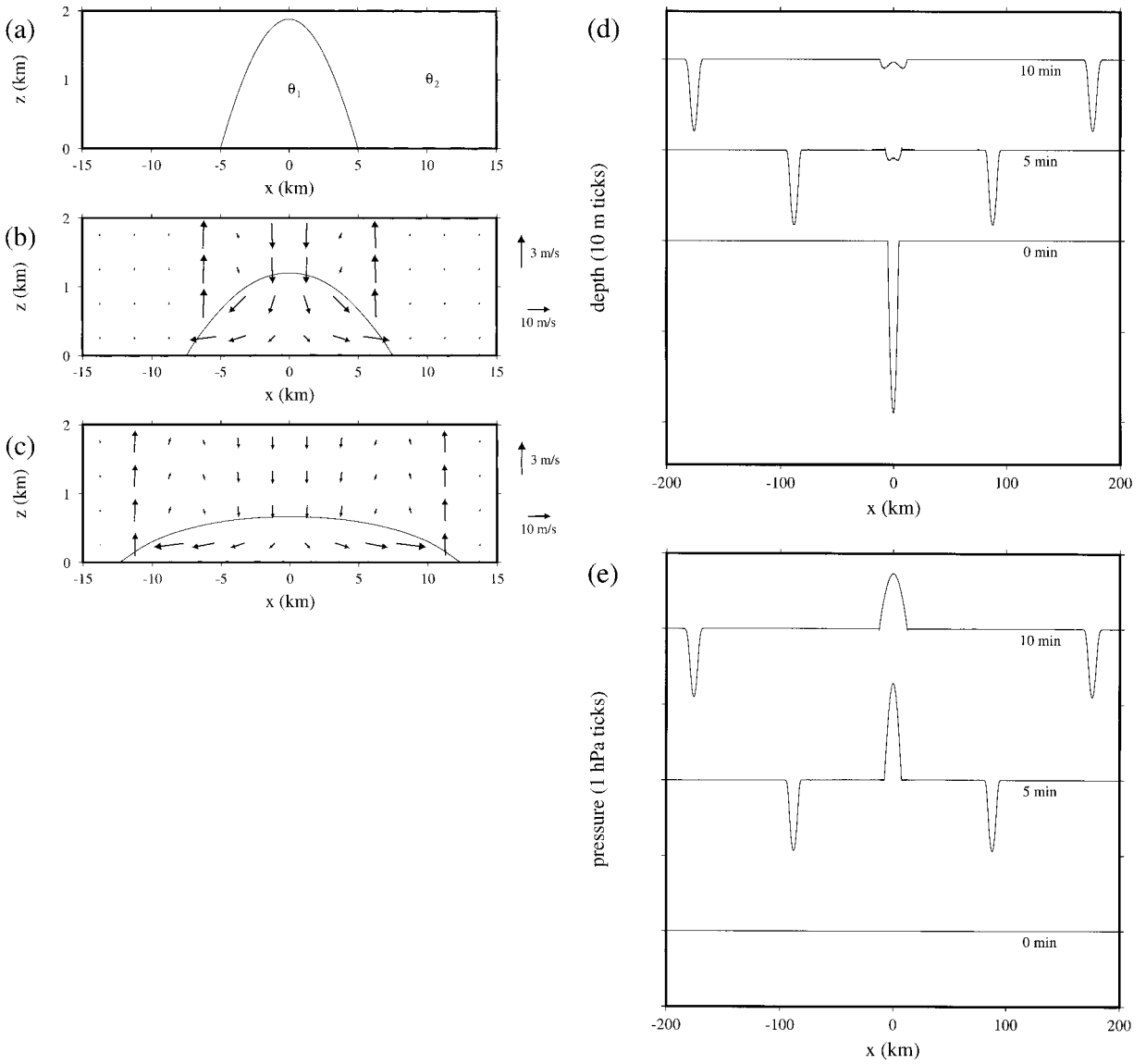

FIG. 3. The outflow that is a gravity current at (a) 0 min, (b) 5 min, and (c) 10 min. (d) Time series of the perturbation depth of the atmosphere. The undisturbed value is 30 734.7 m, and successive curves are displaced by 10 m. (e) Time series of perturbation surface pressure. The undisturbed value is 1000 hPa, and successive curves are displaced by 2 hPa.

cause the cooling occurs instantly; if the cooling were to take place over just 1 min the pressure drop would be one-fourth as intense. When the gust front reaches the observer at 7 min, the pressure begins to rise (Fig. 4a), the temperature drops (Fig. 4b), and there is a sudden wind surge (Fig. 4c).

b. The gravity wave

Now consider an atmosphere that comprises two isentropic layers with potential temperatures of $\theta_1 = 297$ K and $\theta_2 = 300$ K. Suppose that the surface pressure is initially 1000 hPa and that the lower layer has one-fifth the mass of the upper layer. Suppose that a thunderstorm instantly cools a portion of the upper layer to a potential temperature of θ_1. Once again we assume that the region of cooled air has a horizontal scale of 10 km and a maximum fractional column mass of one-fifth (Fig. 5a). The depth perturbation in the lower layer divides into two gravity waves (Figs. 5b,c). By 10 min the leading edge of each wave is about 13 km away from the center of the cooling, and each wave has an amplitude of 940 m. The maximum horizontal velocity is about 5 m s^{-1}, and vertical velocities exceed 3 m s^{-1} in the upper layer just ahead of the waves. There is return flow within the upper layer of the waves so that the entire wave circulation may be described as a roll (Figs. 5b,c).

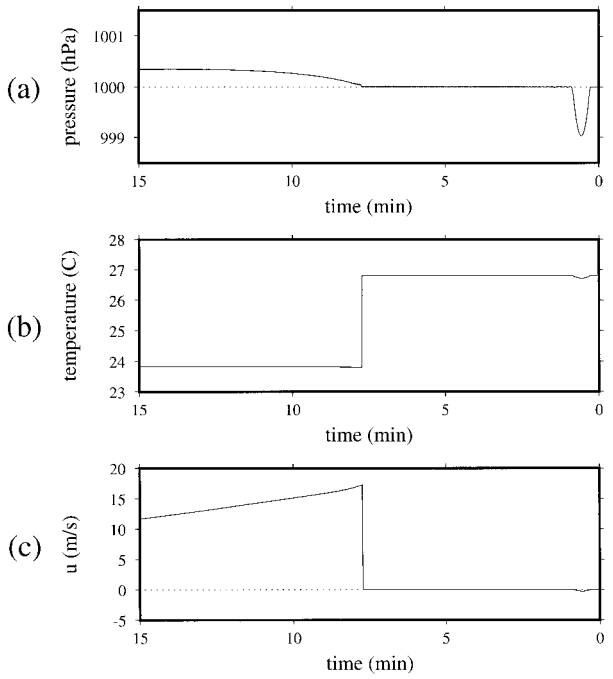

FIG. 4. Measurements of the gravity-current outflow taken by a hypothetical observer at $x = 10$ km: (a) pressure, (b) temperature, and (c) velocity.

As in the previous simulation the cooling causes a perturbation in the depth of the entire atmosphere that divides into two waves that rapidly propagate away (not shown). The surface pressure is initially undisturbed, (Fig. 5d) and after the slow- and fast-moving waves disperse their respective signals are evident. Low pressure accompanies the fast-moving waves and high pressure accompanies the slow-moving waves so that the local surface-pressure field develops a double-hump structure by 5 min (Fig. 5d).

Regarding the previous simulation, the terms ''outflow'' and ''cool air'' may be used interchangeably, and each gust front is accompanied by a temperature fall. In this case, however, the material surface that bounds the cooler air does not intersect the ground (Figs. 5a–c), and there is almost no temperature variation near the ground. Nevertheless, there are still gust fronts, that is, regions where surface winds change rapidly on the leading edges of the outflow (located at $x = -9$ and $x = 9$ km in Fig. 5b). Unlike those in the previous simulation these gust fronts are not advected; they propagate. Consider the movement of parcel X (Figs. 5a–c). It is initially located at the edge of the cooling, and the gust front propagates through it eventually leaving it motionless several kilometers away from its original position.

Suppose again that an observer is standing at $x = 10$ km with meteorological instruments. As in the previous simulation at 30 s the observer measures a trough in surface pressure (Fig. 6a) accompanied by weak signals in temperature (Fig. 6b) and wind (Fig. 6c). The gust front passes between 5 and 9 min, and both pressure and velocity increase significantly, but there is little change in temperature. Just as in the previous simulation the surface-pressure rise is caused by a temperature perturbation in the lower atmosphere. In this case, however, it is elevated (e.g., note the change in potential tem-

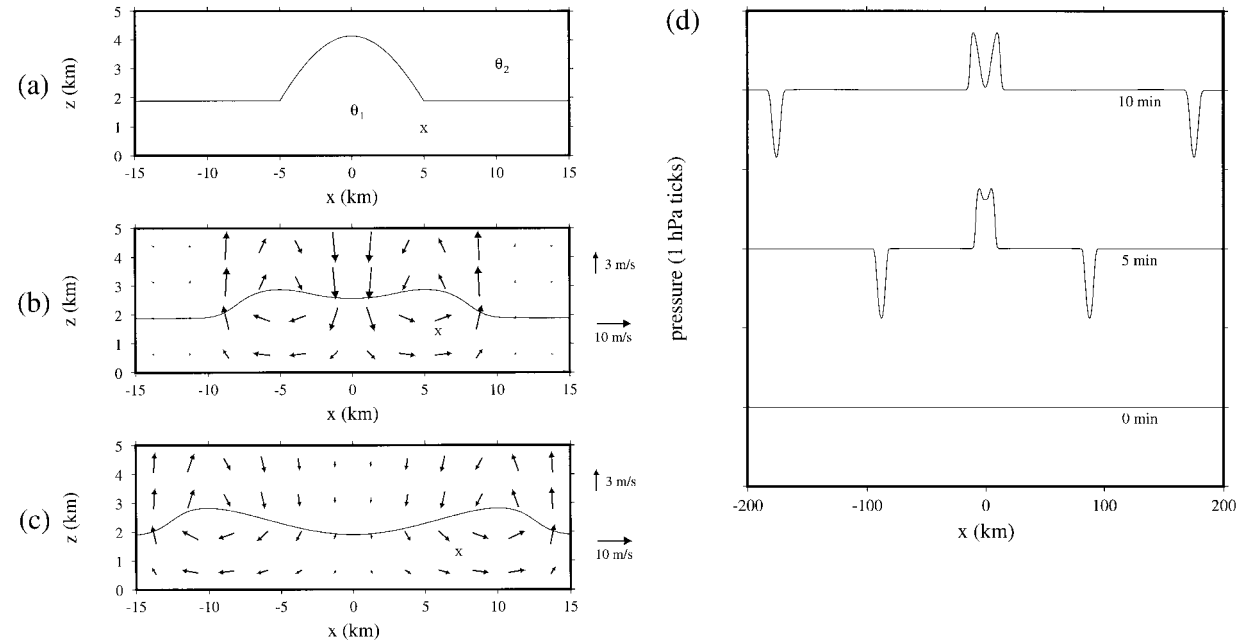

FIG. 5. The outflow that is a gravity wave at (a) 0 min, (b) 5 min, and (c) 10 min. The trajectory of parcel X is marked. (d) Time series of perturbation surface pressure. The undisturbed value is 1000 hPa, and successive curves are displaced by 2 hPa.

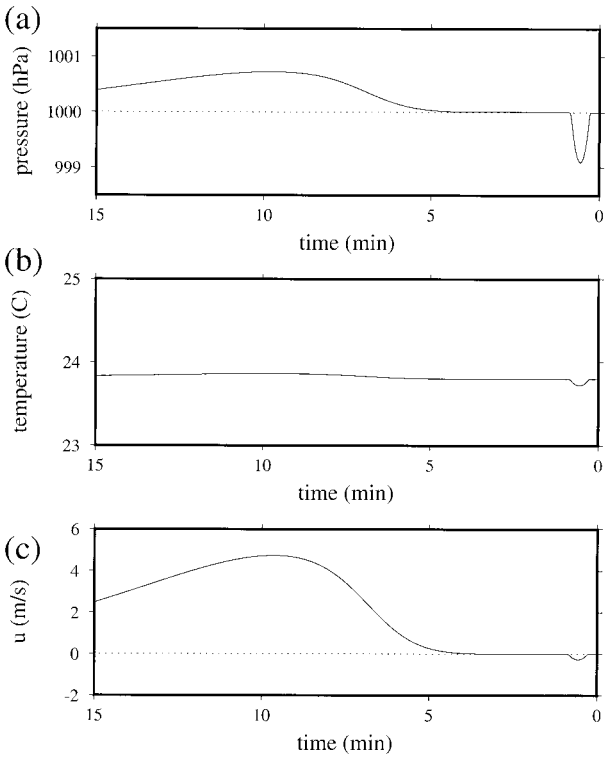

FIG 6. Measurements of the gravity wave outflow taken by a hypothetical observer at $x = 10$ km: (a) pressure, (b) temperature, (c) velocity.

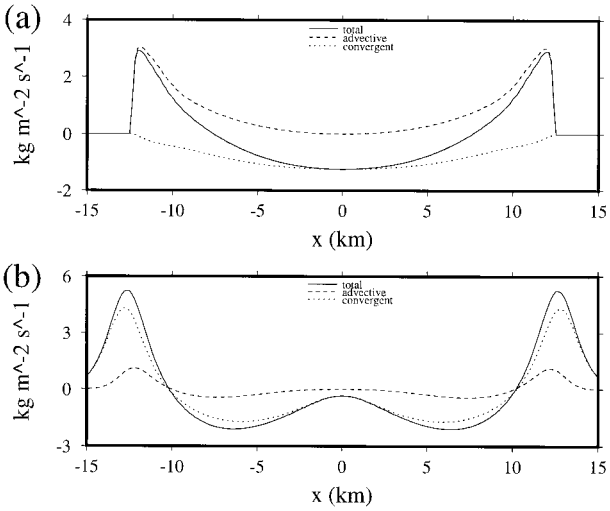

FIG. 7. The time rate of change of the mass of the lower layer ($\partial m_1/\partial t$, solid) at 10 min partitioned into components associated with horizontal advection ($-u_1 \partial m_1/\partial x$, dashed) and convergence ($-m_1 \partial u_1/\partial x$, dotted) for the (a) gravity current and (b) gravity wave.

perature at $x = 10$ km, $z = 2.5$ km between 5 and 10 min in Fig. 5), and it is more a consequence of vertical advection than of horizontal advection.

Although this simulation only directly applies to a thunderstorm outflow forming in an environment containing a sharp low-level inversion, the response of a continuously stratified atmosphere to a low-level cooling is similar. Gravity waves propagate away from the cooling and are accompanied by positive surface pressure perturbations and elevated negative temperature perturbations, with no temperature change at the surface (Haertel and Johnson 2000).

c. The dynamical distinction

As each of the gravity-current and gravity wave gust fronts pass the observer the mass per unit area of the lower layer of the atmosphere increases with time. The nature of this mass increase is different for the two outflows, however. For the gravity-current outflow it is attributable to advection, and for the gravity wave outflow it is primarily attributable to convergence. In this section we discuss this distinction between the two outflows.

The continuity equation for the lower layer of the atmosphere may be rewritten as follows:

$$\frac{\partial m_1}{\partial t} = -u_1 \frac{\partial m_1}{\partial x} - m_1 \frac{\partial u_1}{\partial x}. \tag{11}$$

The local tendency of mass per unit area may be partitioned into two terms, one associated with horizontal advection [the first term on the righthand side of (11)], and the other associated with horizontal convergence [the second term on the righthand side of (11)]. Each of these terms is plotted for each outflow at 10 min in Fig. 7. The mass per unit area is increasing at the leading edges of the gravity-current outflow owing to advection; the convergent term is slightly negative there (Fig. 7a). In contrast, the increase in mass per unit area at the leading edges of the gravity wave outflow is primarily caused by convergence (Fig. 7b). Perhaps this should be the defining dynamical distinction between the two kinds of outflows.

While few people would would argue with our characterization of the first outflow as a gravity current and the second outflow as a gravity wave, one can imagine an outflow within a two-layer atmosphere that is not clearly one or the other. Suppose we were to repeat the second simulation reducing the mass in the lower layer of the undisturbed atmosphere. At some point the advection of mass would become comparable to the convergence of mass on the leading edges of the outflow and the outflow would have characteristics of both a current and a wave. Therefore the two outflow simulations represent two points on a continuum; the gravity-current outflow lies at one end of the continuum, and the gravity wave outflow lies toward the other end.

The term ''bore'' has been used to describe a number of thunderstorm outflows. We have for the most part avoided this term, and now we explain why. Locatelli et al. (1998) define a bore as ''a propagating disturbance

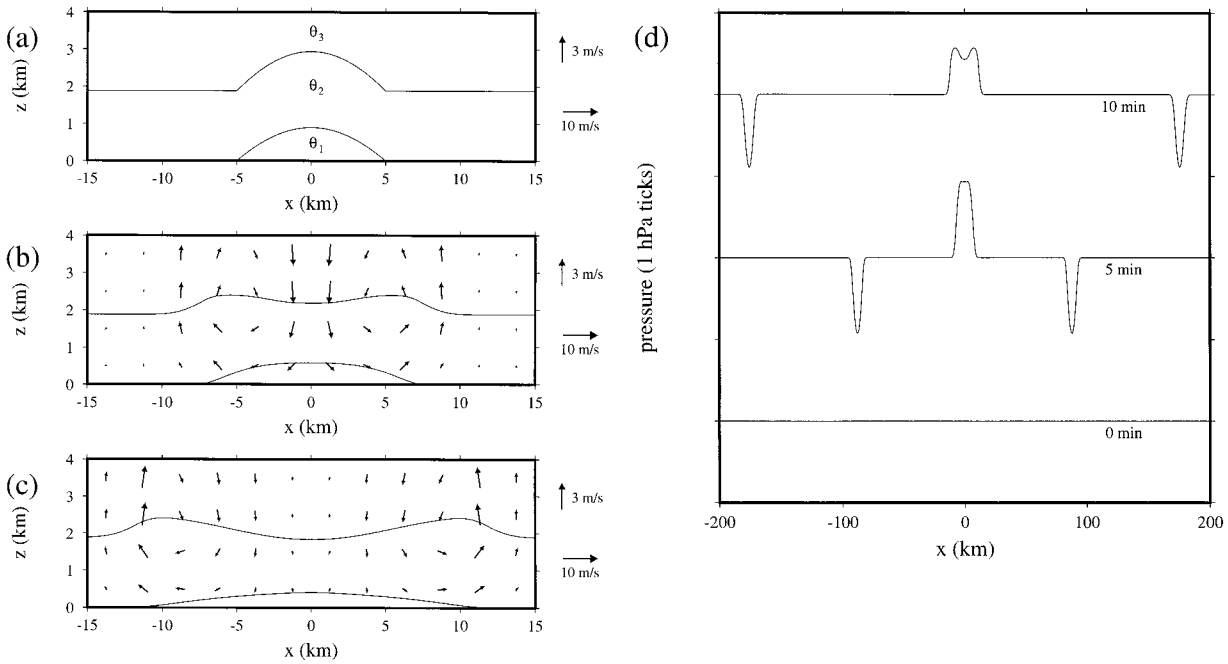

FIG. 8. The outflow that is a gravity current/wave at (a) 0 min, (b) 5 min, and (c) 10 min. (d) Time series of perturbation surface pressure. The undisturbed value is 1000 hPa, and successive curves are displaced by 2 hPa.

that is characterized by a sudden, and relatively permanent, change in the height of a horizontal fluid interface and in the velocity of the fluid beneath the interface.'' According to this definition, a broad, gravity wave outflow with a steep leading edge would be considered a bore, as would a gravity-current outflow spreading into a region with a very shallow layer of air having the same entropy as the outflow. These two types of disturbances differ dynamically; the propagation of the former is attributable primarily to the convergence of mass, whereas the advection of mass drives the advance of the latter. Indeed, laboratory and theoretical studies of bores support the idea that strong bores behave like gravity currents and weak bores behave like gravity waves (Rottman and Simpson 1989; Klemp et al. 1997). We avoid ''bore'' because we wish to distinguish between these differing dynamical entities.

d. The gravity current/wave

We have already mentioned that an outflow in a two-layer atmosphere might lie near the middle of the gravity-current–gravity wave continuum. In this section we present a simulation of a different kind of outflow that exhibits characteristics of both a wave and a current.

Suppose that the atmosphere comprises two isentropic layers with potential temperatures of $\theta_2 = 297$ K and $\theta_3 = 300$ K. Now suppose that a thunderstorm instantly cools a portion of the lower layer to $\theta_1 = 294$ K and a portion of the upper layer to θ_2 (Fig. 8a). Once again we assume that horizontal scale of the cooling is 10 km, and that the maximum fractional column mass of the cooled air is one-fifth. As in the first simulation the coolest air subsides and spreads with time (Figs. 8b,c). As in the third simulation the perturbation in the depth of the second layer divides into two gravity waves that propagate away. By 10 min the gravity waves and the gravity current combine to cause a double-hump structure in the surface pressure field (Fig. 8d).

For this case the observer notices the pressure beginning to rise and the wind beginning to change several minutes before the temperature falls (Figs. 9a–c). In other words the gravity wave arrives ahead of the gravity current. When the gravity current arrives a sudden wind change accompanies a temperature fall, just as in the first simulation.

e. Nonhydrostatic pressure

By using the hydrostatic approximation we are able to greatly simplify the dynamical system that describes the evolutions of the idealized outflows. We cannot justify this approximation by saying that nonhydrostatic pressure is neglibible; for the initial conditions and time periods considered here perturbation nonhydrostatic pressure gradients are about half as intense as perturbation hydrostatic pressure gradients. Our rationale for using the hydrostatic system is philosophical. We wish to illustrate some of the most fundamental outflow dynamics in their simplest form. Having done this we now consider how nonhydrostatic pressure alters the simulations.

We repeat each of the simulations using the Advanced Regional Predicition System (www.caps.ou.edu/ARPS).

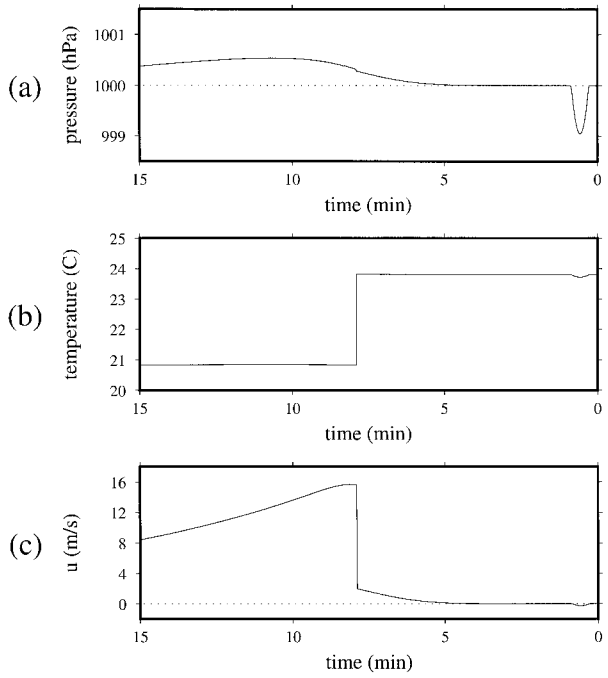

FIG. 9. Measurements of the gravity-current–wave outflow taken by a hypothetical observer at $x = 10$ km: (a) pressure, (b) temperature, (c) velocity.

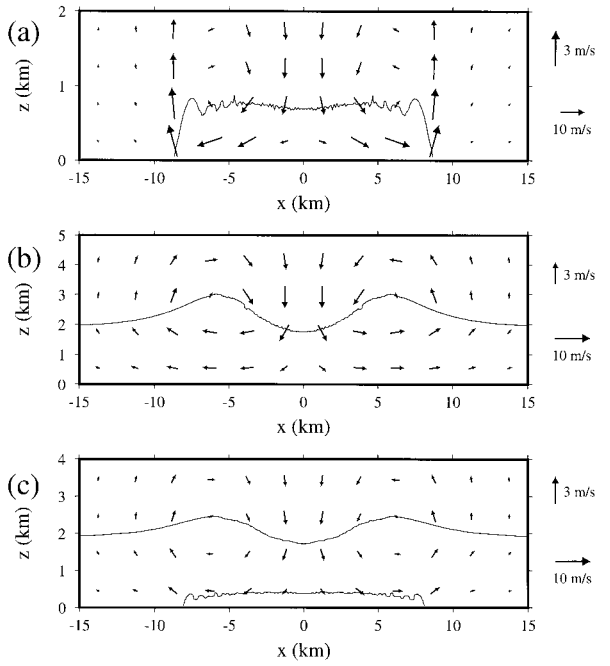

FIG. 10. Nonhydrostatic simulations of (a) gravity-current, (b) gravity wave, and (c) gravity-current/wave outflows at 10 min. The 298.5 K theta surface is contoured in (a)–(b), and the 295.5 K and 298.5 K theta surfaces are contoured in (c).

We use fourth-order advection of scalars and momentum with flux-corrected transport, ∇^2 diffusion with a mixing coefficient of 1 $m^2\ s^{-1}$, vertical and horzontal grid spacings of 100 m, rigid horizontal and vertical boundaries at 25 and 10 km, respectively, and time splitting with a large time step of 1 s and a small time step of 0.2 s.

At 10 min the nonhydrostatic outflow circulations are qualitatively and quantitatively similar to their hydrostatic counterparts, but they advance more slowly (Figs. 3c, 5c, 8c, 10a–c). The nonhydrostatic gravity current has a more vertical leading edge, and a head is just starting to develop at this time (Fig. 10a). The nonhydrostatic gravity waves have steeper trailing edges and flatter leading edges (Figs. 10b). The nonhydrostatic gravity-current–wave exihibits each of these differences (Figs. 10c).

A pressure decomposition for the nonhydrostic gravity-current–wave outflow reveals why the nonhydrostatic outflows advance more slowly (Figs. 11a–c). Beneath the waves there are nonhydrostatic lows (Fig. 11c), and in the vicinity of these lows the horizontal nonhydrostatic pressure gradient works against the horizontal hydrostatic pressure gradient (Fig. 11b). This is consistent with gravity wave theory, which predicts a smaller phase velocity for nonhydrostatic waves than for hydrostatic waves, especially for short waves (e.g., Gill 1982, Fig. 5.5b, p. 103). There is also a nonhydrostatic high-low couplet centered on the leading edge of each gravity current (Fig. 11c) similar to that observed by Droegemeier and Wilhelmson (1987), and the

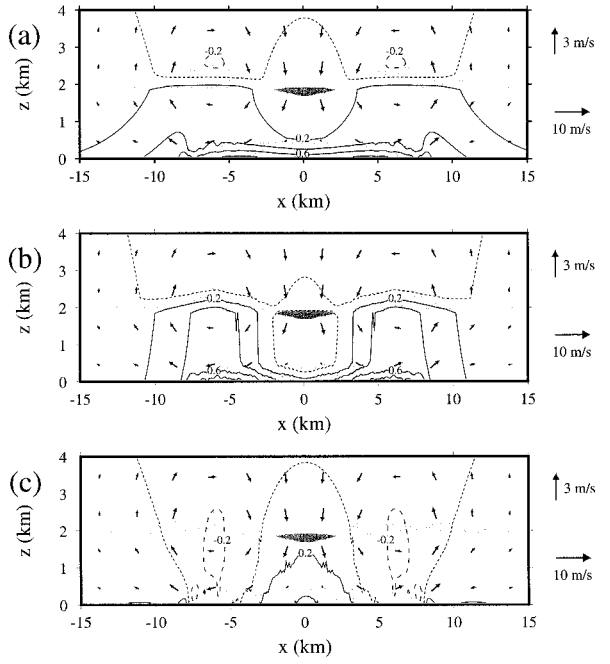

FIG. 11. Pressure contours and wind vectors for the gravity-current/wave outflow at 10 min. (a) Total pressure perturbation, (b) hydrostatic pressure perturbation, (c) and nonhydrostatic pressure perturbation. Positive contours are solid, zero contours are dotted, negative contours are dashed, and the contour interval is 0.2 hPa. Regions with temperature perturbations of more than 1 K in magnitude are shaded, light for negative perturbations, and dark for positive perturbations.

gradient associated with this couplet retards the advance of the gravity current. This gradient appears to have done more to slow the current by this time than momentum transport by Kelvin-Helmholz billows (Mueller and Carbone 1987), which are just starting to become active at 10 min.

Although the greatest surface pressure occurs several kilometers behind the leading edge of each gravity current, high pressure does extend ahead of the current for several km (Fig. 11a). This high is largely a hydrostatic manifestation of the gravity wave, but nonhydrostatic pressure adds to it (Figs. 11b,c).

The dynamical distinction we noted earlier between the hydrostatic gravity-current and gravity wave outflows also exists between the nonhydrostatic gravity-current and gravity wave outflows. Let h denote the height of the 298.5 K theta surface (we consider this surface to separate the upper and lower layers). The mass per unit area m of the lower layer is as follows:

$$m = \int_0^h \rho \, dz. \tag{12}$$

Applying Leibniz's rule yields:

$$\frac{\partial m}{\partial t} = \int_0^h \frac{\partial \rho}{\partial t} \, dz + \frac{\partial h}{\partial t}(\rho)_h. \tag{13}$$

By the continuity equation we have $\partial\rho/\partial t = -\partial(\rho u)/\partial x - \partial(\rho w)/\partial z$ and since the 298.5 K theta surface is a material surface we have $\partial h/\partial t = (w)_h - (u)_h \partial h/\partial x$. Substituting into (13) and using the fact that the vertical mass flux vanishes at $z = 0$, we obtain

$$\frac{\partial m}{\partial t} = (\rho u)_h \frac{\partial h}{\partial x} - \int_0^h u \frac{\partial \rho}{\partial x} \, dz - \int_0^h \rho \frac{\partial u}{\partial x} \, dz. \tag{14}$$

The first two terms in the righthand side of (14) are associated with horizontal advection and the third term is associated with horizontal convergence. Just as in the hydrostatic simulations, the increases in the mass per unit area at the leading edges of the gravity-current outflow are primarily caused by advection (Fig. 12a), whereas mass increases associated with the gravity wave gust fronts are caused primarily by convergence (Fig. 12b). However, for the nonhydrostatic gravity-current outflow, convergence is also significant 1–2 km back from the leading edges (Fig. 12a). This convergence produces a head on the gravity current that is just starting to become apparent at 10 min (Fig. 10a) and is more pronounced at 15 min (not shown).

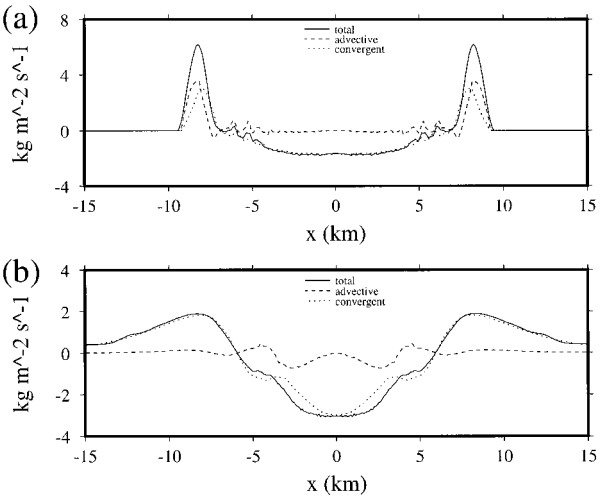

FIG. 12. The time rate of change of the mass of air with potential temperature less than 298.5 K at 10 min partitioned into components associated with horizontal advection (dashed) and convergence (dotted) for the (a) nonhydrostatic gravity-current outflows and (b) nonhydrostatic gravity wave outflows.

4. Summary and discussion

Within each of the simulations presented here a portion of the lower atmosphere is cooled, having its potential temperature reduced by 3 K. For each case the same amount of mass is cooled and the horizontal distribution of cooling is the same. What differs among the simulations are the initial states of the atmosphere and the vertical distributions of the cooling. As a consequence of these differences the outflows differ dynamically. The first two simulations illustrate two fundamental types of outflows, the gravity current and the gravity wave. They are distinguished by how they advance. The leading edges of the gravity-current outflow are advected, whereas the gravity wave outflow propagates owing to horizontal convergence. The gravity current–wave simulation illustrates that low-level cooling may also generate an outflow that is a combination of these fundamental types. When nonhydrostatic pressure is included in the simulations the outflows have similar circulations, but they advance more slowly. Nonhydrostatic surface-pressure highs develop ahead of the gravity currents, but they are smaller in scale and in magnitude than the hydrostatic highs associated with the gravity waves.

The distinction between gravity wave and gravity-current outflows has not always been recognized in previous studies; gravity wave outflows are often treated as gravity currents. For example, compare two of the outflows identified as gravity currents in the seminal work by Wakimoto (1982). The afternoon 17 June outflow exhibited characteristics of a gravity current: 1) a sudden temperature drop and sharp wind shift accompanied the gust front (Fig. 13a); 2) the outflow spread into a weakly stratified environment (Fig. 13b); 3) the lowest 1.2 km of the atmosphere cooled when the gust front passed (Fig. 13b), and radar measurements indicated that the outflow was 1.1 km deep just before it passed the sounding station (Wakimoto 1982, Fig. 7), so that the depth of the outflow and the cooling were consistent. The 16 June 1978 outflow, on the other hand, exhibited characteristics of a gravity wave: 1) The gust front was accompanied by a pressure rise that occurred

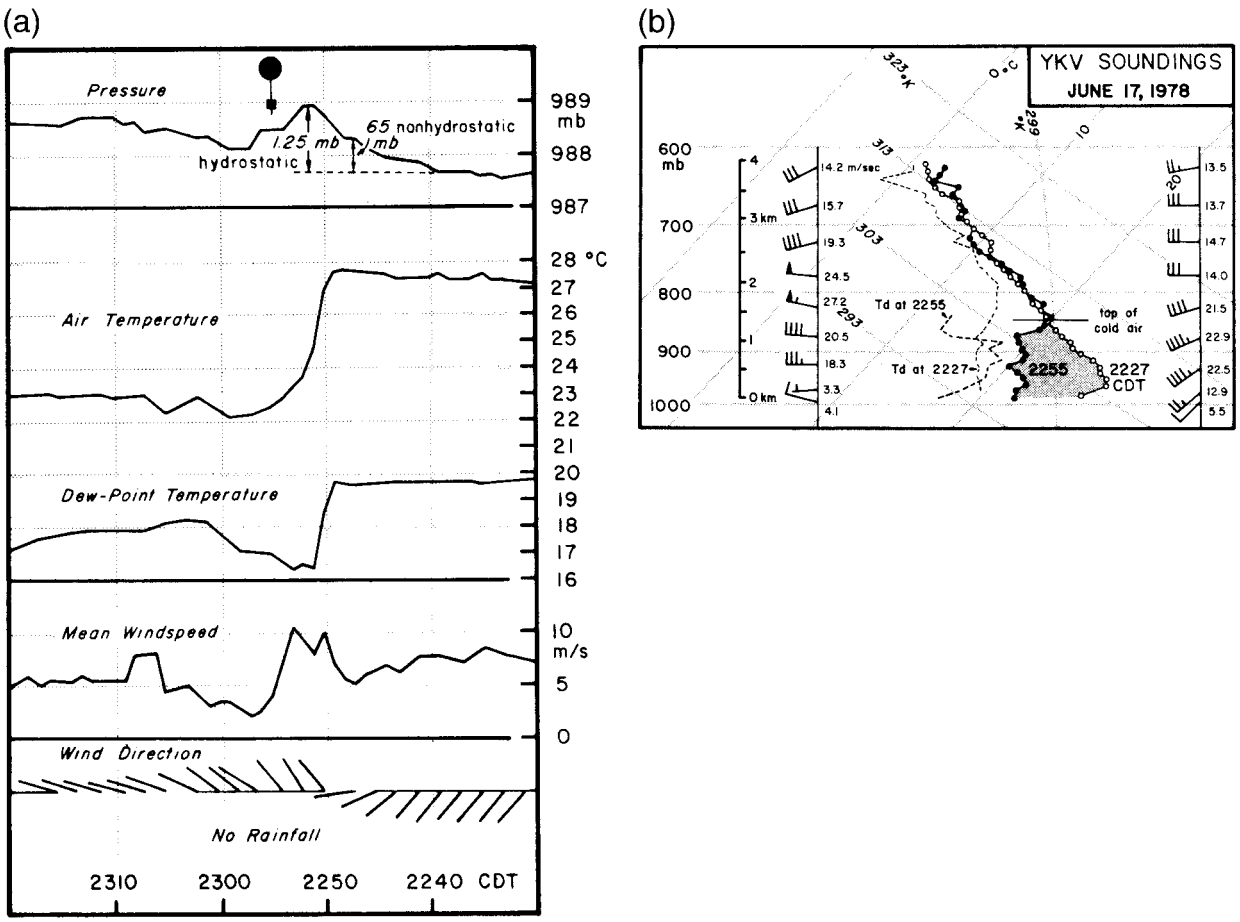

FIG. 13. The afternoon 17 Jun 1978 outflow (from Wakimoto 1982): (a) surface measurements. The time of a sounding is marked with a balloon symbol. (b) Soundings before and after the passage of the gust front.

over 30 min in phase with a steady change in the surface wind vector with little change in surface temperature (Fig. 14a); 2) the outflow spread into a strongly stratified environment (Fig. 14b); 3) the lowest 4 km of the atmosphere cooled when the gust front passed (Fig. 14b), and the outflow was about 2 km deep just before it passed the sounding station (Wakimoto 1982, Fig. 13), so that the depth of the cooling and the outflow were not consistent; 4) the observed rate of gust front motion (20 m s^{-1}) was very close to theoretical value (18 m s^{-1}) for a gravity wave with a half vertical wavelength of 4 km given the observed Brunt–Väisällä frequency (about 0.014 s^{-1}). While characteristic 3 would also be expected for a modified gravity current (Haase and Smith 1989), the remaining characteristics point to the 16 June outflow being a gravity wave.

The gravity current/wave simulation illustrates that the high in surface pressure commonly observed ahead of gravity-current outflows (e.g., Fig 13a), which has generally been labeled as a nonhydrostatic high, may in some cases be a hydrostatic manifestatation of a gravity wave. While there is no evidence of such wave in the sounding taken after the passage of the afternoon 17 outflow (Fig. 13b), surface pressure had fallen somewhat before this sounding was taken (Fig. 13a), and it is possible that a wave had already passed by this time. Koch et al. (1991) provide a rare time-continuous thermodynamic profile of an outflow (Fig. 15), and the many undulations in theta surfaces suggest substantial gravity wave activity.

As a final point we note that while previous studies of thunderstorm outflows having gravity wave–bore components have suggested that the bore–wave component was generated by the interaction of the gravity current with a stable layer, it is possible in some such cases that a bore–wave is generated directly by low-level cooling. Consider the gravity current–wave simulation presented here. If the cooling of the lower layer (gravity current) were removed but the cooling of the upper layer retained, the gravity wave would remain. So in this case the gravity wave is generated by low-level cooling and modified by the gravity current.

Acknowledgments. This research was supported by the National Science Foundation under Grants ATM-9618684 and ATM-9812384. The authors thank three

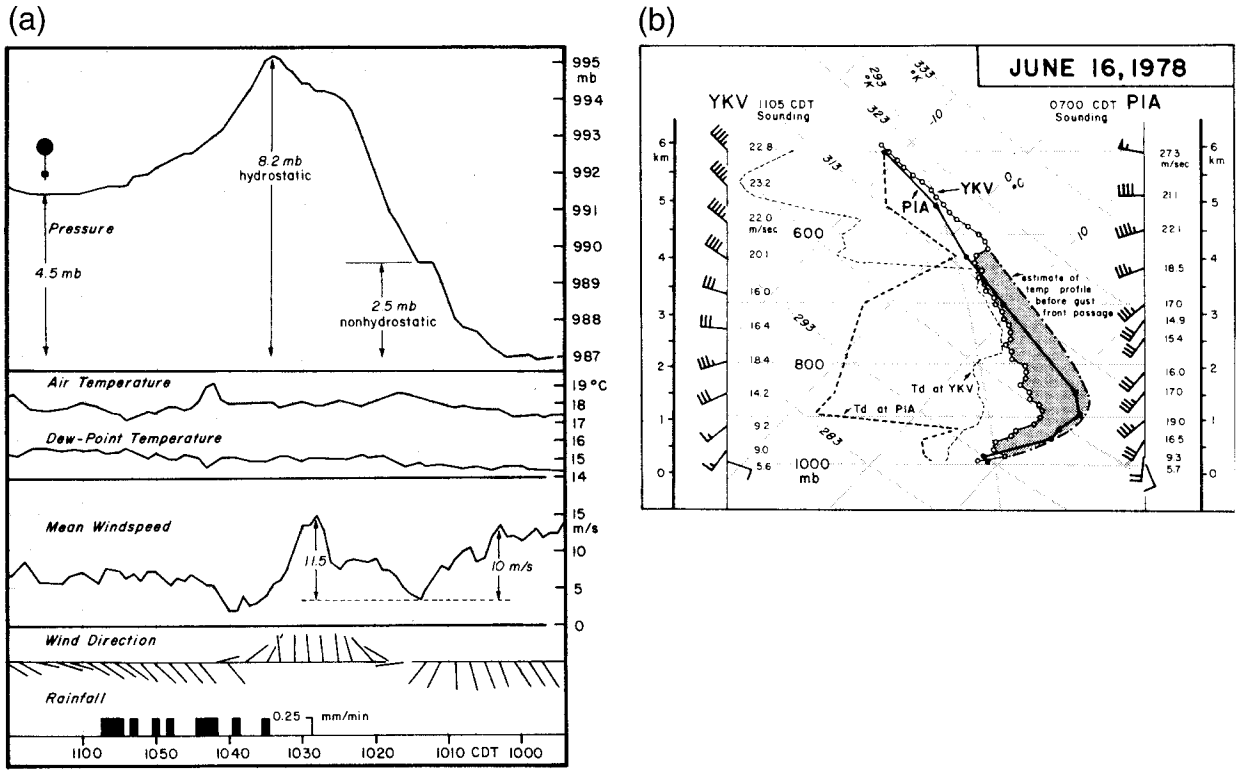

FIG. 14. The 16 Jun 1978 outflow (from Wakimoto 1982): (a) surface measurements. The time of a sounding is marked with a balloon symbol. (b) An estimated sounding before the passage of the gust front and an actual sounding taken after the passage of the gust front.

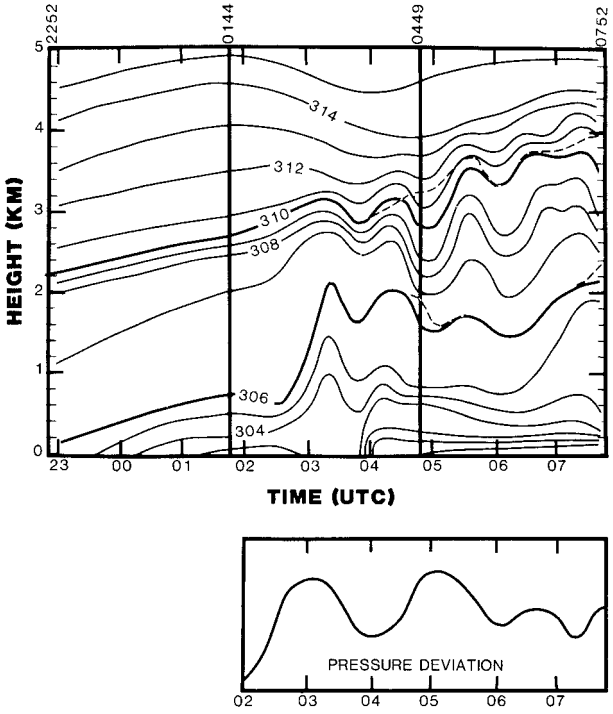

FIG. 15. The 8–9 Jun 1987 outflow (from Koch et al. 1991). A time series of potential temperature inferred from (upper) lidar measurements and (lower) surface pressure.

anonymous reviewers and Michael Montgomery for their comments and suggestions. The nonhydrostatic simulations were carried out using the Advanced Regional Prediction System (ARPS) developed by the Center for Analysis and Prediction of Storms (CAPS), University of Oklahoma. CAPS is supported by the National Science Foundation and the Federal Aviation Administration through combined Grant ATM92-20009.

REFERENCES

Benjamin, T. B., 1968: Gravity currents and related phenomena. *J. Fluid Mech.,* **31,** 209–248.

Charba, J., 1974: Application of gravity current model to analysis of squall-line gust front. *Mon. Wea. Rev.,* **102,** 140–156.

DeMaria, M., and J. D. Pickle, 1988: A simplified system of equations for simulation of tropical cyclones. *J. Atmos. Sci.,* **45,** 1542–1554.

Doviak, R. J., and R. Ge, 1984: An atmospheric solitary gust observed with a Doppler radar, a tall tower and a surface network. *J. Atmos. Sci.,* **41,** 2559–2573.

Droegemeier, K. K., and R. B. Wilhelmson, 1987: Numerical simulation of thunderstorm outflow dynamics. Part I: Outflow sensitivity experiments and turbulence dynamics. *J. Atmos. Sci.,* **44,** 1180–1210.

Frei, C., 1993: Dynamics of a two-dimensional ribbon of shallow water on an f-plane. *Tellus,* **45A,** 44–53.

Fulton, R., 1990: Initiation of a solitary wave family in the demise of a nocturnal thunderstorm density current. *J. Atmos. Sci.,* **47,** 319–337.

Gill, A. E., 1982: *Atmosphere–Ocean Dynamics.* Academic Press, 662 pp.

Goff, R. C., 1976: Vertical structure of thunderstorm cutflows. *Mon. Wea. Rev.,* **104,** 1429–1440.

Haase, S. P., and R. K. Smith, 1989: The numerical simulation of atmospheric gravity currents. Part II: Environments with stable layers. *Geophys. Astrophys. Fluid Dyn.,* **46,** 35–51.

Haertel, P. T., and R. H. Johnson, 2000: The linear dynamics of squall line mesohighs and wake lows. *J. Atmos. Sci.,* **57,** 93–107.

Klemp, J. B., R. Rotunno, and W. C. Skamarock, 1994: On the dynamics of gravity currents in a channel. *J. Fluid Mech.,* **269,** 169–198.

——, ——, and ——, 1997: On the propagation of internal bores. *J. Fluid Mech.,* **331,** 81–106.

Koch, S. E., P. B. Dorian, R. Ferrare, S. H. Melfi, W. C. Skillman, and D. Whiteman, 1991: Structure of an internal bore and dissipating gravity current as revealed by Raman lidar. *Mon. Wea. Rev.,* **119,** 857–887.

Locatelli, J. D., M. T. Stoelinga, P. V. Hobbs, and J. Johnson, 1998: Structure and evolution of an undular bore on the high plains and its effect on migrating birds. *Bull. Amer. Meteor. Soc.,* **79,** 1043–1060.

May, P. T., 1999: Thermodynamic and vertical velocity structure of two gust fronts observed with wind profiler/RASS during MCTEX. *Mon. Wea. Rev.,* **127,** 1796–1807.

Mueller, C. K., and R. E. Carbone, 1987: Dynamics of a thunderstorm outflow. *J. Atmos. Sci.,* **44,** 1879–1898.

Rottman, J. W., and J. E. Simpson, 1989: The formation of internal bores in the atmosphere: A laboratory model. *Quart. J. Roy. Meteor. Soc.,* **115,** 941–963.

Schär, C., and P. K. Smolarkiewicz, 1996: A synchronous and iterative flux-correction formalism for coupled transport equations. *J. Comput. Phys.,* **128,** 101–120.

Tao, X., 1994: Wave mean flow interaction and stratospheric sudden warmings in and isentropic model. *J. Atmos. Sci.,* **51,** 134–153.

Wakimoto, R. M., 1982: The life cycle of thunderstorm gust fronts as viewed with Doppler radar and rawinsonde data. *Mon. Wea. Rev.,* **110,** 1060–1082.